

# Vapochromic Luminescent $\pi$ -Conjugated Systems with Reversible Coordination-Number Control of Hypervalent Tin(IV)-Fused Azobenzene Complexes

Masayuki Gon,<sup>[a]</sup> Kazuo Tanaka,<sup>\*[a]</sup> and Yoshiki Chujo<sup>[a]</sup>

**Abstract:** The dynamic and reversible changes of coordination numbers between five and six in solution and solid states, based on hypervalent tin(IV)-fused azobenzene (TAz) complexes, are reported. It was found that the TAz complexes showed deep-red emission owing to the hypervalent bond composed of an electron-donating three-center four-electron (3c–4e) bond and an electron-accepting nitrogen–tin (N–Sn) coordination. Furthermore, hypsochromic shifts in optical spectra were observed in Lewis basic solvents because of alteration of the coordination number from five to six. In

particular, vapochromic luminescence was induced by attachment of dimethyl sulfoxide (DMSO) vapor to the coordination point at the tin atom accompanied with a crystal–crystal phase transition. Additionally, the color-change mechanism and degree of binding constants were well explained by theoretical calculation. To the best of our knowledge, this is the first example of vapochromic luminescence by using stable and variable coordination numbers of hypervalent bonds.

## Introduction

Vapochromic luminescent properties are the class of stimuli-responsive phenomena where compounds change luminescent color by exposing solvent vapor.<sup>[1,2]</sup> Development of organic materials are strongly required for realizing intelligent optoelectronic organic devices, such as chemical sensors because tuning of optical properties including luminescent colors is expectable by chemical modification and substituent effects.<sup>[3]</sup> Vapochromic luminescence is usually regarding induction of inter- or intramolecular structural changes with  $\pi$ -conjugated systems.<sup>[4–14]</sup> In many cases, the luminescence-color change is triggered by insertion of solvent molecules into the crystal structure as guest molecules. By modifying with organic bulky substituents and long alkyl chains which are capable of causing drastic structural rearrangements of molecular distributions by solvent absorbing, electronic structures at the luminophores are critically perturbed. The limited examples of the vapochromic luminescence are caused by the direct attachment of solvent molecules to the metal center in the luminescent complexes.<sup>[15–27]</sup> In this approach, transition metal complexes have been often used for capturing vapor molecules. Transition metals can readily change the valence number and subsequently show different optical properties in each state. If stable coordination states can be constructed, desired behaviors are obtained. Thus, it is desired for constructing tailor-made color-

tuning systems to realize next generation of optoelectronic sensors.

Heteroatom-containing building blocks are effective in constructing functional and unique materials.<sup>[28–30]</sup> As examples, we discovered cubic silica and boron cluster compounds named polyhedral oligomeric silsesquioxane (POSS)<sup>[31,32]</sup> and *o*-carborane,<sup>[33,34]</sup> respectively, have been applicable to main scaffolds for creating functional materials showing superior luminescence behaviors with high durability or stimuli-responsiveness. We recently reported the series of solid-state luminescent complexes and polymers containing boron-fused azomethine ( $-\text{C}=\text{N}-$ )<sup>[35–39]</sup> and azo ( $-\text{N}=\text{N}-$ )<sup>[40–44]</sup> complexes with the tridentate ligands, *o*-salicylideneaminophenol or 2,2'-dihydroxyazobenzene scaffold, respectively.<sup>[45]</sup> These materials showed intense emission in the condensed state, and highly-efficient polymer film emission<sup>[38]</sup> and near-infrared (NIR) absorptive and emissive characteristics<sup>[40–42,44]</sup> were obtained. It should be emphasized that unique environment-sensitive luminescent properties, such as aggregation-induced emission (AIE),<sup>[46,47]</sup> crystallization-induced emission enhancement (CIEE),<sup>[48]</sup> in which enhanced emission can be observed only in aggregation and crystal, respectively. Thus, we regarded these complexes as a solid-state luminescent building block having stimuli-responsivity.

Herein, we illustrate that the hypervalent tin(IV)-fused azobenzene (TAz) complexes are the robust platform for realizing color-tunable vapochromic luminescent  $\pi$ -conjugated systems. To the best of our knowledge, we found that TAz systems can show enough stability for isolation and structural analyses of both five and six coordinated structures and reactivity to offer the first example of color-tunable vapochromic luminescence based on the dynamic and reversible coordination-number changes. We synthesized the series of the TAz complexes and found the formation of five coordinated

[a] Dr. M. Gon, Prof. Dr. K. Tanaka, Prof. Dr. Y. Chujo  
Department of Polymer Chemistry  
Graduate School of Engineering,  
Kyoto University  
Katsura, Nishikyo-ku, Kyoto 615-8510 (Japan)  
E-mail: tanaka@poly.synchem.kyoto-u.ac.jp

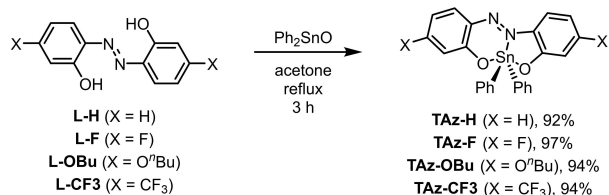
Supporting information for this article is available on the WWW under <https://doi.org/10.1002/chem.202100571>

structures with the distorted trigonal bipyramidal geometry.<sup>[49,50]</sup> Additionally, the **TAz** complexes exhibited emission in the deep-red regions both in solution and solid states owing to the hypervalent bond of tin atom including an electron-donating three-center four-electron (3c–4e)<sup>[51]</sup> bond and an electron-accepting nitrogen-tin (N–Sn) coordination. Moreover, it was shown that hypsochromic luminescence was observed in the presence of some kinds of Lewis basic solvents. In particular, the dimethyl sulfoxide (DMSO)-coordinated complexes showed high stability enough for further structural and optical analyses, and it was revealed that chromism and luminochromism originating from the coordination number changes from five to six at the tin atom. The binding affinities followed by vapochromic luminescent behaviors were varied by the substituent effect in the azobenzene ligand. Moreover, the order of binding constants measured in solution and the color-change mechanism based on the  $\pi$ -conjugated system were good explained by theoretical investigation. In other words, from the theoretical calculations, it should be possible to estimate not only binding constants but also vapochromic luminescence behaviors in this system. Finally, by using the powder samples, we can demonstrate good reversibility. This is the first example, to the best of our knowledge, to offer color-tunable vapochromic luminescence based on the dynamic and reversible changes of the coordination number in the hypervalent tin complexes.

## Results and Discussion

### Synthesis

Scheme 1 shows the syntheses of the **TAz** complexes with hydrogens (**TAz-H**), halogens (**TAz-F**), electron-withdrawing groups (**TAz-CF<sub>3</sub>**) and electron-donating groups (**TAz-OBu**). All of the complexes were prepared by the reaction between azobenzene tridentate ligands and diorganotin(IV) oxide under reflux conditions with acetone in almost quantitative yields.<sup>[49]</sup> The ligand, 2,2'-dihydroxyazobenzene (**L-H**), is commercially available, and the detailed synthetic methods for the other ligands (**L-F**, **L-CF<sub>3</sub>** and **L-OBu**) and model compounds, **Az-H**, **Az-F**, **Az-OBu**, **Az-CF<sub>3</sub>**, are described in the Supporting Information. The structures of new compounds in this study were confirmed by <sup>1</sup>H, <sup>13</sup>C and <sup>119</sup>Sn NMR spectroscopies, high-resolution mass spectrometry (HRMS), and elemental analyses. From these characterization data, we concluded that the products should have desired structures with high purity



**Scheme 1.** Synthesis of **TAz** complexes from each ligand.

enough for structural and optical measurements. It should be noted that all products show good stability to light, air and moisture in solution and solid, meaning that degradation should be negligible in further analyses.

### NMR spectra

The structures of **TAz** complexes in solution were investigated with <sup>1</sup>H, <sup>13</sup>C and <sup>119</sup>Sn NMR spectrometry. From <sup>1</sup>H and <sup>13</sup>C NMR spectra in chloroform-*d* (CDCl<sub>3</sub>), the signal peaks attributable to five- and six-membered rings were clearly detected. According to the previous reports, the fast conformational change of the coordination position at the N=N bond in the azobenzene ligand, called as a “pedal motion”,<sup>[52]</sup> is proposed in the silicon-azobenzene complexes.<sup>[53,54]</sup> In our study, because both benzene rings were distinguishable in <sup>1</sup>H and <sup>13</sup>C NMR spectra at high temperature (Figure S1), structural fluctuation might be ignorable even in solution. The chemical shifts of <sup>119</sup>Sn NMR spectra (–365.4 ppm for **TAz-H**, –366.5 ppm for **TAz-F**, –367.3 ppm for **TAz-OBu** and –360.2 ppm for **TAz-CF<sub>3</sub>**) were similar to that of the five coordinated tin atom with two phenyl groups (–328.4 ppm).<sup>[55]</sup> Interestingly, the large upfield shifts in the <sup>119</sup>Sn NMR spectra were observed in DMSO-*d*<sub>6</sub> (–467.3 ppm for **TAz-H**, –471.1 ppm for **TAz-F**, –465.0 ppm for **TAz-OBu** and –475.9 ppm for **TAz-CF<sub>3</sub>**, Figure S2), strongly suggesting that the DMSO coordination should proceed at the tin atom followed by the formation of the six coordinated state.<sup>[56–59]</sup> This result also means that the asymmetric five- and six-coordinated structures can be obtained by selecting the solvent between CDCl<sub>3</sub> and DMSO-*d*<sub>6</sub>, respectively. Noted that the complexes involving six-coordinated states showed high stability. Therefore, we tried isolation of these DMSO-coordinated complexes.

### Crystal structures

The structures of the **TAz** complexes were confirmed by single crystal X-ray diffraction (SC-XRD) analyses (Figures 1A and S3–S6). Representative bond lengths, angles and dihedral angles are listed in the distorted trigonal bipyramidal geometry (Table S1).<sup>[49]</sup> The formation of the five-coordinated tin atom is proved from the structural data. Around the tin atom, two oxygen atoms (O(1) and O(2)) were at the apical positions, and nitrogen (N(1) or N(2)) and two carbon atoms in the phenyl groups (C(13) and C(19)) were at the equatorial positions. The angles of O(1)–Sn(1)–O(2) were 157.5° for **TAz-H**, 159.3° for **TAz-F**, and 157.8° for **TAz-CF<sub>3</sub>**, indicating that the structural distortion should be involved (ideal angle, 180°). The dihedral angles of C(1)–N(1)–N(2)–C(7) were –179.3° for **TAz-H**, –178.7° for **TAz-F** and –179.5° for **TAz-CF<sub>3</sub>** and the azobenzene moieties were highly planar regardless of substituent effects. The bond lengths of N(1)–N(2) were 1.26 Å for **TAz-H**, 1.25 Å for **TAz-F** and 1.27 Å for **TAz-CF<sub>3</sub>**. These values were within a category of the N=N bond of azobenzene (1.25–1.27 Å).<sup>[49,60]</sup> The structure of **TAz-OBu** was not able to be determined due to large disorders at linear butyl chains (Figure S5). Regarding the

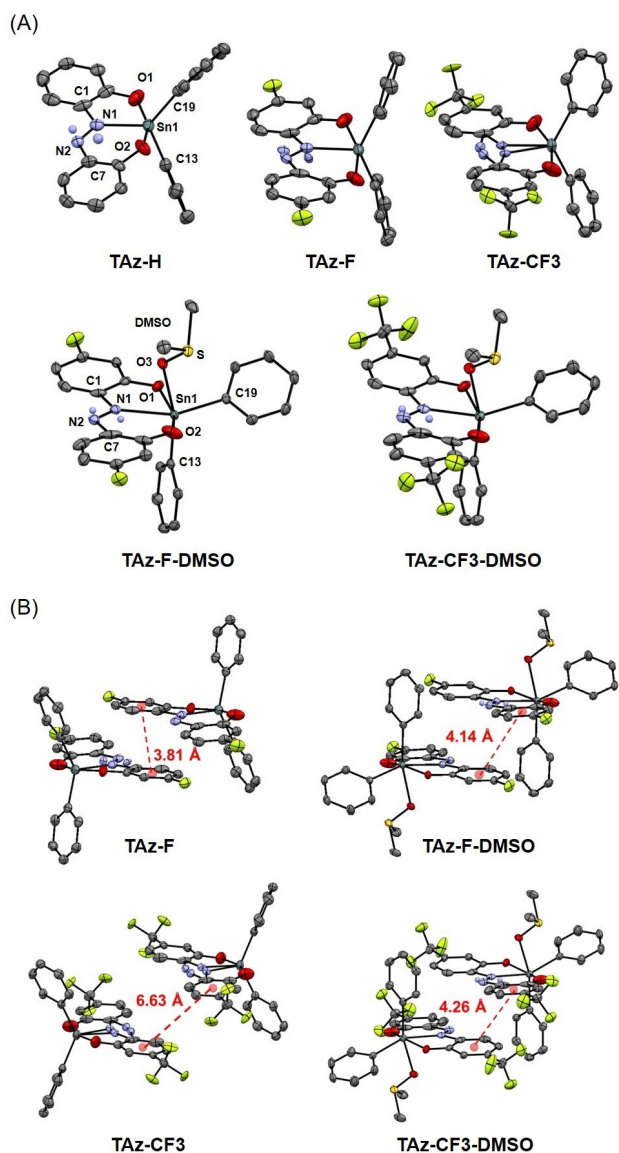


**Figure 1.** (A) ORTEP drawings of TAz-H, TAz-F, TAz-CF<sub>3</sub>, TAz-F-DMSO and TAz-CF<sub>3</sub>-DMSO (50% probability for thermal ellipsoids). (B) Crystal packing structures of TAz-F and TAz-F-DMSO, TAz-CF<sub>3</sub> and TAz-CF<sub>3</sub>-DMSO with the distances of the closest two benzene rings. Hydrogen and a part of disordered atoms are omitted to clarify. All crystallographic data are shown in the Supporting Information.

ambiguity of the nitrogen atoms, two different nitrogen positions in crystal packings were detected from the complexes, especially TAz-CF<sub>3</sub>. This result implies that existence of a “pedal motion” might occur in crystal.<sup>[52–54,61]</sup> Meanwhile, the NMR data suggest that the conformational changes should hardly proceed even in solution. Therefore, we assume that the ambiguity of nitrogen positions in the crystalline state should be categorized in a static disorder,<sup>[52]</sup> not a dynamic one, which is caused by the difficulty in the distinguishment of both structures replaced the five- and six-membered rings from each other in the SC-XRD analysis.

Fortunately, in the case of TAz-F and TAz-CF<sub>3</sub>, we successfully isolated the single crystals of the six-coordinated

tin complexes with the DMSO coordination.<sup>[57]</sup> The crystals were sufficiently grown in the saturated DMSO solutions of TAz-F and TAz-CF<sub>3</sub>. Figures 1A, S8 and S9 show ORTEP drawings of the obtained DMSO complexes, TAz-F-DMSO and TAz-CF<sub>3</sub>-DMSO. Representative bond lengths, angles and dihedral angles are also listed in Table S1. The oxygen atom of DMSO was perpendicularly attached to the tin atom against the azobenzene surface and formed an orthogonal geometry.<sup>[55]</sup> The angles of O(1)–Sn(1)–O(2), dihedral angles of C(1)–N(1)–N(2)–C(7) and the bond lengths of N(1)–N(2) were 155.1°, –177.6° and 1.25 Å for TAz-F-DMSO, 155.5°, –176.8° and 1.25 Å for TAz-CF<sub>3</sub>-DMSO, respectively. These values mean that the geometry of the azobenzene ligand is hardly changed during the transition between five and six coordination states. That is,  $\pi$ -planarity, which is the origin of luminescence, should be preserved after the coordination. The DMSO attachment induced a slight bond elongation of Sn(1)–N(1), Sn(1)–C(13) and Sn(1)–C(19) (+0.10 Å, +0.04 Å and +0.02 Å from TAz-F, +0.10 Å, +0.05 Å and +0.03 Å from TAz-CF<sub>3</sub>, respectively), suggesting that bond strengths could be released by the DMSO coordination. Although the single crystal of TAz-H-DMSO was obtained, the unit cell was too large to obtain reliable crystal data (Figure S7). The difficulty in obtaining a distinct crystal packing structure of TAz-H-DMSO is probably because there were no dimeric interactions between DMSO moieties as seen in TAz-F-DMSO and TAz-CF<sub>3</sub>-DMSO (Figures S8B and S9B). In addition, there are few effects of the donor and acceptor substituents or DMSO attachments on the distribution of the  $\pi$ -electrons because distinct alteration of the bond lengths of benzene rings in azobenzene moiety was hardly observed among TAz complexes (Figure S10). In summary, critical structural changes influenced on the optical properties, such as distortion of  $\pi$ -planes, were hardly induced by the DMSO coordination.

Another structural feature is the distances between each molecule in the crystalline cell, which critically influence emission efficiency in solid. Most of luminescent organic dyes show poor luminescence in solid due to intermolecular interaction, and this concentration quenching process is one of critical issues to be solved for obtaining luminescent materials and devices.<sup>[46,62]</sup> Therefore, it is known that condensed molecular distribution is unfavorable for receiving emission in the solid state. From the crystal of TAz-F, relatively tight packing was obtained (3.81 Å), whereas the much longer intermolecular distance was observed from TAz-CF<sub>3</sub> (6.63 Å) (Figure 1B). The sparse packing is favorable for obtaining solid-state luminescence by suppressing concentration quenching. Surprisingly, by the DMSO coordination, the opposite changes were observed. The longer distance was detected by +0.33 Å from TAz-F, meanwhile the close packing was obtained in the TAz-CF<sub>3</sub>-DMSO crystal (–2.37 Å). These changes in molecular distribution would play a critical role in emission efficiency in solid.

### Solution-state UV-vis absorption measurements

Firstly, UV-vis absorption spectra of the **TAz** complexes were measured in solution for investigating electronic structures in the ground state (Figures 2, S11 and Tables 1, S11–S13). Azobenzene derivatives are known to show a strong  $\pi$ - $\pi^*$  transition band around 370 nm and a weak  $n$ - $\pi^*$  band around 450 nm,<sup>[61]</sup> while the tin complexes showed the absorption bands attributed to  $\pi$ - $\pi^*$  transition in the longer wavelength region (500 nm~). This means that drastic stabilization effects on electronic structures are obtained by the tin coordination.<sup>[44,49,63]</sup> Thus, the **TAz** complexes can have a narrow energy gap despite that this molecule has small-sized  $\pi$ -conjugated system. The detailed mechanism will be discussed later with the theoretical calculation data.

Interestingly, hypsochromic shifts of the absorption bands were observed by the DMSO coordination. As representative examples, comparing to the spectra in  $\text{CHCl}_3$  and DMSO/ $\text{CHCl}_3=99/1$  v/v solutions ( $1.0 \times 10^{-5}$  M), we found that the absorption bands were blue-shifted in the presence of DMSO (Figures 2 and S12). The shapes and positions of the absorption bands were hardly changed in hexane, toluene,  $\text{CHCl}_3$  and

dichloromethane ( $\text{CH}_2\text{Cl}_2$ ) which are classified into non-coordinating solvents (Figure S11A). Meanwhile, clear hypsochromic shifts in the absorption spectra in the series of coordinating (Lewis basic) solvents, such as tetrahydrofuran (THF), 1,4-dioxane, ethyl acetate (EtOAc), acetone, ethanol (EtOH), acetonitrile (MeCN), dimethyl formamide (DMF) and DMSO, were observed, indicating that these solvents can drastically perturb electronic structures of the azobenzene ligands by the coordination to tin atom (Figure S11B). From the structural analyses as shown in previous section (Figure 1), significant changes in the  $\pi$ -plane were not obtained. Therefore, it is proposed that electronic properties at the tin atom should be responsible for these band shifts. It is noteworthy that the solvent-coordinated **TAz** complexes hardly showed any degradation under ambient conditions. Stable six-coordinated complexes were able to be obtained. Furthermore, as demonstrated later, the coordination and detachment can reversibly proceed without degradation. These stability of both hypervalent states are advantageous in the usages as practical sensors.<sup>[64]</sup>

### Photoluminescence

To examine electronic structures in the excited state, emission properties were evaluated. In photoluminescence (PL) spectra, the bands of the **TAz** complexes were observed from orange to NIR regions (Figures 3, S13 and Table 1). The emission properties were largely affected by the substitution effects.<sup>[63,65]</sup> The peak top wavelengths ( $\lambda_{\text{PL}}$ ) in  $\text{CHCl}_3$  were obtained in the red region. Larger emission efficiencies ( $\Phi_{\text{PL}}$ ) were observed from **TAz-F** and **TAz-OBu**. To obtain further information on emission mechanisms, we estimated radiative and non-radiative rate constants ( $k_r$  and  $k_{\text{nr}}$ ) from lifetime measurements (Figure S14). Relatively smaller  $k_r$  and larger  $k_{\text{nr}}$  were observed **TAz-H**. Significant differences in the substituent effect were hardly obtained between the electron-donating (**TAz-OBu**) and accepting groups (**TAz-F**). It is suggested that  $\pi$ -conjugation effects in relation to delocalization of the lone-pair electrons of fluorine or oxygen atoms seem to be positive for enhancing emission. This is because expansion of  $\pi$ -conjugation should increase transition probability and structural rigidity which lead to rising the value of  $k_r$  and reducing the value of  $k_{\text{nr}}$ , respectively.

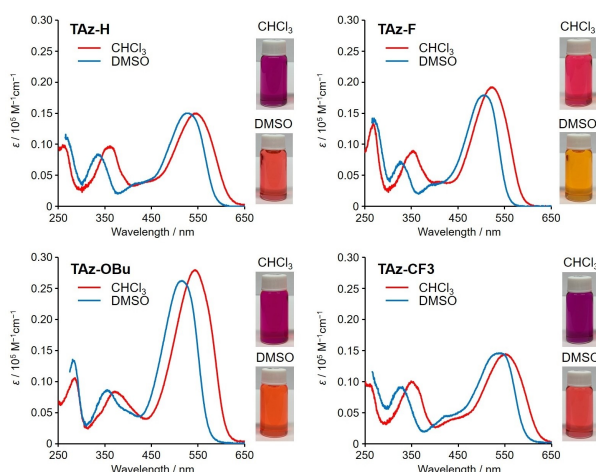


**Figure 2.** UV-vis absorption spectra and photos under room lights of **TAz-H**, **TAz-F**, **TAz-OBu** and **TAz-CF3** ( $1.0 \times 10^{-5}$  M) in  $\text{CHCl}_3$  (red line) and DMSO/ $\text{CHCl}_3=99/1$  v/v (blue line). The concentration of the samples of photos were  $5.0 \times 10^{-5}$  M for clear recognition of color differences.

	Solvent	$\lambda_{\text{abs}}/\text{nm}$	$\lambda_{\text{PL}}^{[c]}/\text{nm}$	$\Phi_{\text{PL}}^{[c]}$	$\tau^{[d]}$ ( $\alpha$ )/ns	$k_r^{[e]}/10^8 \text{ s}^{-1}$	$k_{\text{nr}}^{[e]}/10^8 \text{ s}^{-1}$
<b>TAz-H</b>	$\text{CHCl}_3$	547	678	0.035	0.74	0.47	13
	DMSO <sup>[b]</sup>	528	626	0.041	0.69	0.59	14
<b>TAz-F</b>	$\text{CHCl}_3$	523	640	0.21	3.1	0.69	2.6
	DMSO <sup>[b]</sup>	506	596	0.032	0.34 (89%) 1.9 (11%)	0.34	10
<b>TAz-OBu</b>	$\text{CHCl}_3$	543	643	0.33	3.1	1.0	2.2
	DMSO <sup>[b]</sup>	515	622	0.32	2.7	1.2	2.6
<b>TAz-CF3</b>	$\text{CHCl}_3$	551	681	0.057	1.0	0.55	9.2
	DMSO <sup>[b]</sup>	538	638	0.012	0.16 (57%) 1.2 (43%)	0.12	9.9

[a]  $1.0 \times 10^{-5}$  M. [b] In mixed solvent, DMSO/ $\text{CHCl}_3=99/1$  v/v. [c] Absolute PL quantum efficiency excited at  $\lambda_{\text{abs}}$ . [d] PL lifetime monitored at  $\lambda_{\text{PL}}$ . [e]  $k_r = \Phi_{\text{PL}}/\tau_{\text{av}}$ ,  $k_{\text{nr}} = (1 - \Phi_{\text{PL}})/\tau_{\text{av}}$ ,  $\tau_{\text{av}} = \sum \alpha_i \tau_i^2 / \sum \alpha_i \tau_i$ ,  $\alpha$ : relative amplitude.

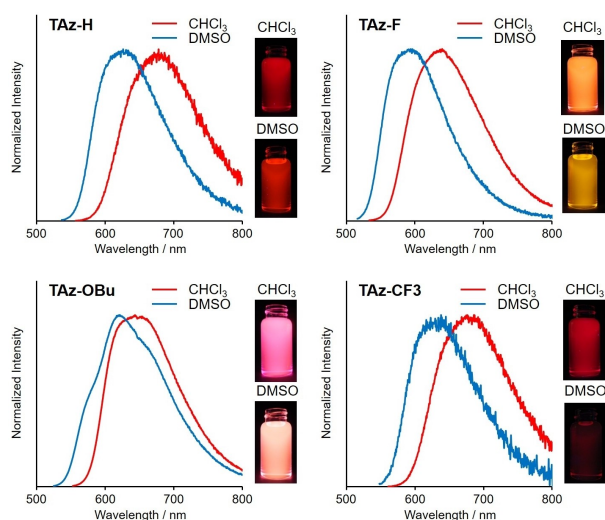


**Figure 3.** PL spectra and photos irradiated by a UV lamp (365 nm) of **TAz-H**, **TAz-F**, **TAz-OBu** and **TAz-CF3** in  $\text{CHCl}_3$  (red line) and  $\text{DMSO}/\text{CHCl}_3 = 99/1$  v/v (blue line), excited at wavelengths of absorption maxima. The concentration of the samples of photos were  $5.0 \times 10^{-5}$  M for clear recognition of color differences.

In  $\text{DMSO}/\text{CHCl}_3 = 99/1$  v/v solution, hypsochromic shifts in the PL spectra were also detected in all **TAz** complexes, similarly to the absorption spectra (Figure 3). After the  $\text{DMSO}$  coordination, intense emissions with high  $\Phi_{\text{PL}}$ s were still observed. These data mean that the  $\text{DMSO}$  coordination should be retained in the excited state. If the  $\text{DMSO}$  detachment occurred in the excited state, the emission components of the five coordinated system should be observed with large bathochromic effect accompanied with drastic structural relaxation. That is,  $\text{DMSO}$  detachment is negligible in the photoluminescence processes. According to the orders of  $\lambda_{\text{PL}}$  and  $\Phi_{\text{PL}}$  values, it was found that the electron-withdrawing groups lowered emission efficiencies. In addition, this tendency was observed in the other solvents (Tables S9–S12). Furthermore, the smaller  $k_{\text{r}}$ s and larger  $k_{\text{nr}}$ s, which are negative tendencies for giving luminescence, were detected after the  $\text{DMSO}$  coordination especially in **TAz-F** and **TAz-CF3** (Table 1). In comparison to only  $\pi$ -conjugation effects in the absence of  $\text{DMSO}$ , luminescent properties of the hypervalent tin complexes can be influenced by the substituent effect. These results suggest that tuning of optical properties is acceptable in this system.

### Binding constants

The crystal structures obtained from SC-XRD analyses indicated 1:1 binding between the five coordinated **TAz** complex and  $\text{DMSO}$ . To investigate whether the same 1:1 binding occurs in solution, we carried out titration experiments (Figures S15–S22) and variable temperature (VT) measurements (Figure S23) of absorption in toluene/ $\text{DMSO}$  mixed solutions. The results from both of the titration experiments and the VT measurements suggested the existence of the isosbestic points which should

support the existence of the 1:1 binding. Moreover, the VT measurements proved that the alteration between the five and six coordination states can reversibly proceed without significant degradation. On the basis of these analyses, we estimated a binding constant ( $K$ ) in 1:1 binding with the results of titration experiments (Table 2). Accordingly, the  $K_{\text{DMSO}}$  values of the complexes were calculated as  $3.9 \text{ M}^{-1}$  for **TAz-H**,  $6.6 \text{ M}^{-1}$  for **TAz-F**,  $1.3 \text{ M}^{-1}$  for **TAz-OBu** and  $25 \text{ M}^{-1}$  for **TAz-CF3** (Figures S15–S18). As suggested in the PL measurements in the presence and absence of  $\text{DMSO}$ , it was also shown that the electron-withdrawing groups tended to enhance binding ability. We also calculated the binding constant with DMF ( $K_{\text{DMF}}$ ) in the toluene/ $\text{DMF}$  mixed solvent. The values of  $K_{\text{DMF}}$  were estimated to be  $0.55 \text{ M}^{-1}$  for **TAz-H**,  $0.92 \text{ M}^{-1}$  for **TAz-F**,  $0.40 \text{ M}^{-1}$  for **TAz-OBu** and  $3.2 \text{ M}^{-1}$  for **TAz-CF3**, indicating that  $K_{\text{DMF}}$  is much smaller than  $K_{\text{DMSO}}$  (Figures S19–S22). The binding constants of other solvents were too small to be estimated by the titration experiments. The order of binding affinity was similar to the reported Lewis basicity in nonprotogenic solvents by using a zinc Schiff-base complex.<sup>[66]</sup> Therefore, the **TAz** complexes also have a potential to investigate the Lewis basicity by using a tin atom center.

### Cyclic voltammetry

To confirm the narrow-energy-gap properties of the **TAz** complexes, experimental values of HOMO (highest occupied molecular orbital) and LUMO (lowest unoccupied molecular orbital) energy levels were estimated by cyclic voltammetry (Figure S24, Table S13). The HOMO and LUMO energy levels of **TAz-H** were estimated to be  $-5.60$  and  $-3.56$  eV, respectively. On the other hand, those of the methylated ligand, **Az-H**, were calculated to be  $-5.73$  and  $-3.00$  eV, respectively. These results indicate that tin coordination plays a significant role in the elevation of energy levels of HOMO as well as lowering of those of LUMO. The opposite effects by the tin coordination on the energy levels of HOMO and LUMO could originate from position-dependent different natures of the bond properties in the trigonal bipyramidal structure containing 3c–4e bonds at apical positions and  $sp^2$  hybrid orbital at equatorial positions. That is, increases in electron density at the non-bonding orbital of the 3c–4e bond contribute to the enhancement of electron-donating ability of oxygen atoms, leading to elevating the HOMO energy level.<sup>[67,68]</sup> In addition, acceptance of nitrogen electron lone pair by the tin atom decreased the LUMO energy level.<sup>[44]</sup> Consequently, the energy levels of HOMO and LUMO should be independently shifted to the opposite directions. The

Table 2. Binding constants ( $K$ ) of <b>TAz</b> complexes and $\text{DMSO}$ or $\text{DMF}$ . <sup>[a]</sup>		
	$K_{\text{DMSO}}/\text{M}^{-1}$	$K_{\text{DMF}}/\text{M}^{-1}$
<b>TAz-H</b>	3.9	0.55
<b>TAz-F</b>	6.6	0.92
<b>TAz-OBu</b>	1.3	0.40
<b>TAz-CF3</b>	25	3.2

[a] Determined in toluene at ambient temperature.

HOMO and LUMO energy levels of the other **TAz** complexes were  $-5.60$  and  $-3.57$  eV for **TAz-F**,  $-5.23$  and  $-3.38$  eV for **TAz-OBu**,  $-5.78$  and  $-3.88$  eV for **TAz-CF3**, respectively. These data can be explained by the conventional substituent effect, that is, electron-donating and withdrawing groups elevate and lower HOMO and LUMO energy levels, respectively.

### Solid-state coordination

We investigated solid-state optical properties and particularly vapochromism between five and six coordinations. To obtain high sensitivity by enlarging surface areas, we prepared the powder samples through the evaporation with  $\text{CHCl}_3$  solutions. The resulting powders of the **TAz** complexes were exposed by various vapors at ambient temperature with a vapor-saturated closed condition (Figure S25). Almost all samples including doping film in a polymer matrix were dissolved or not changed, meanwhile the color-changed powders were stably obtained in **TAz-F** and **TAz-CF3** with the DMSO vapor (Figure S25). Preservation of DMSO in the crystal packing structure with a dimer should contribute to stable capturing of the solvent vapor.

### PXRD measurements

We carried out a powder X-ray diffraction (PXRD) measurement to confirm the molecular distributions in the powder samples of **TAz-F** and **TAz-CF3** before and after exposure of the DMSO vapor (Figures 4 and S26). In summary, almost identical molecular conformation was obtained between the single crystals and the powder samples both in the presence and absence of DMSO. The pristine samples of **TAz-F** and **TAz-CF3** prepared by evaporation from the  $\text{CHCl}_3$  solutions showed the similar PXRD patterns obtained by the simulations from SC-XRD. After exposure to DMSO, the sample color was clearly varied from dark brown to orange for **TAz-F** and from dark brown to red for **TAz-CF3**. The PXRD patterns were changed to those which were good agreements with the simulated ones with **TAz-F-DMSO** and **TAz-CF3-DMSO**. Furthermore, once the obtained **TAz-F-DMSO** and **TAz-CF3-DMSO** were heated at  $100^\circ\text{C}$ , the sample colors were returned to those at the initial state. The PXRD patterns were almost recovered to the original ones although partial broadening was observed. Those results indicate two important issues. Firstly, the DMSO coordination can proceed even in solid. Secondary, the DMSO coordination and detachment can reversibly proceed with the crystal–crystal transitions. It should be noted that this exposing and heating cycle can be stably repeated at least 3 times (Figure S26). By using powder samples, homogeneous states could be maintained during the cycles.

### Thermogravimetric analysis (TGA)

To estimate the amount of adsorption by DMSO exposure to the powder samples of **TAz-F** and **TAz-CF3**, a thermogravimet-

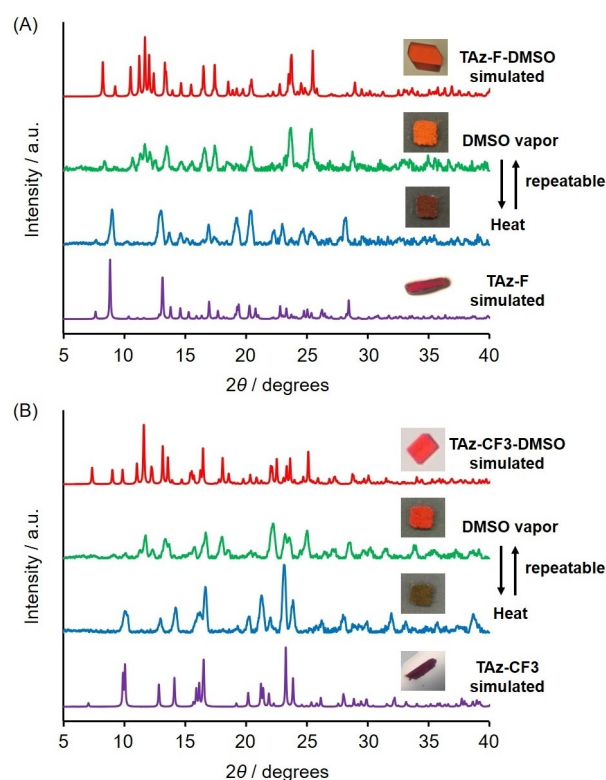


**Figure 4.** PXRD patterns of (A) **TAz-F** and (B) **TAz-CF3** in each state. Purple and red lines show simulated pattern from SC-XRD analyses. Light blue and green lines show the patterns from the heated powder samples at  $100^\circ\text{C}$  for 30 min and exposed samples to DMSO vapor for 4 h at an ambient temperature under a vapor-saturated closed condition, respectively. The inserted photos show the samples in each state under room light.

ric analysis (TGA) was carried out. The samples of **TAz-F-DMSO** and **TAz-CF3-DMSO** were prepared by exposure with the powder samples of **TAz-F** and **TAz-CF3** to saturated DMSO atmosphere for 4 h at ambient temperature under a vapor-saturated closed condition, respectively. The TGA profiles with the single decomposition step were obtained from the pristine samples, whereas two decomposition steps were detected from the DMSO complexes (Figure S27). The first decomposition temperature ( $T_{d1}$ ) and the percentages of weight loss were  $103^\circ\text{C}$  and 12.7 wt% for **TAz-F-DMSO** and  $111^\circ\text{C}$  and 11.6 wt% for **TAz-CF3-DMSO**, respectively (Table S14). These are almost identical to theoretical values calculated from chemical formula, 13.0 wt% for **TAz-F-DMSO** and 11.2 wt% for **TAz-CF3-DMSO**. Therefore,  $T_{d1}$  was attributable to the loss of DMSO. The higher  $T_{d1}$  and fine agreement of DMSO weight loss percentages in **TAz-CF3-DMSO** are corresponded to the larger binding constant than that of **TAz-F-DMSO**.

### Solid-state photoluminescence

We performed PL measurements with the solid samples (Figure 5 and Table 3). Initially, we compared luminescent properties between crystal and powder samples. Larger emission

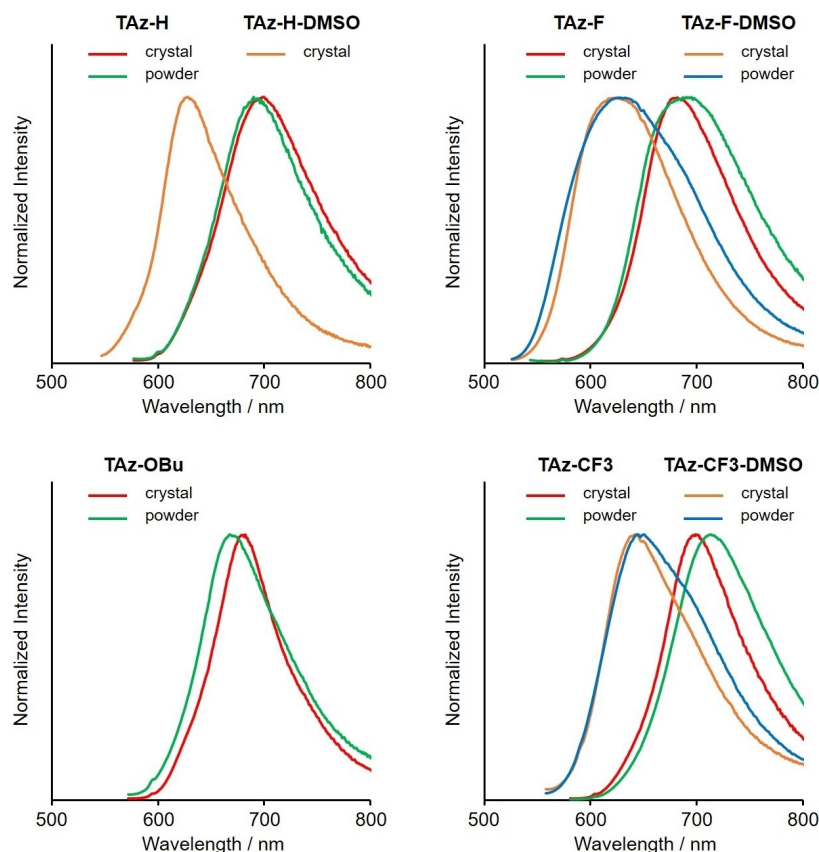


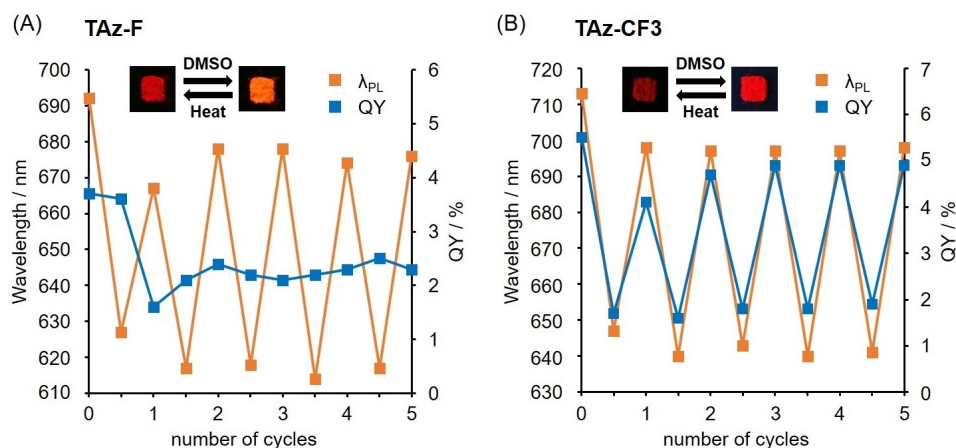
Figure 5. PL spectra of TAZ-H, TAZ-F, TAZ-OBu and TAZ-CF3 in the solid state, excited at wavelengths of absorption maxima under solution conditions.

Table 3. Optical data of the TAZ complexes in solid.				
	Crystal $\lambda_{PL}^{[a]}/nm$	$\Phi_{PL}^{[b]}$	Powder $\lambda_{PL}^{[a]}/nm$	$\Phi_{PL}^{[b]}$
TAz-H	699	0.035	692	0.034
TAz-H-DMSO	628	0.065	— <sup>[c]</sup>	— <sup>[c]</sup>
TAz-F	682	0.044	692	0.023
TAz-F-DMSO	624	0.098	627	0.021
TAz-OBu	680	0.058	667	0.010
TAz-OBu-DMSO	— <sup>[c]</sup>	— <sup>[c]</sup>	— <sup>[c]</sup>	— <sup>[c]</sup>
TAz-CF3	699	0.058	713	0.035
TAz-CF3-DMSO	642	0.021	647	0.013

[a] Excited at absorption maxima in solution ( $\lambda_{abs}$ ). [b] Absolute PL quantum efficiency excited at  $\lambda_{abs}$ . [c] Not isolated as a solid sample.

efficiencies were observed from the crystalline samples than those from the powder ones. It is likely that vigorous molecular tumbling occurs around the surfaces of particles and amorphous regions in the powder samples. Thus, decreases in emission efficiencies were detected from the powder samples although almost the same molecular packing should be formed. However, we performed luminescent vapochromic experiments with the powder samples because of high sensitivity in emission color change and reversibility observed in the chromism investigation. The emission bands with the powder samples were obtained in the deep-red region. By the DMSO exposing under a vapor-saturated closed condition, hypochro-

mic shifts were observed from all samples, similarly to the results with the solution samples. In the powder samples of TAZ-H and TAZ-F, we investigated the reversible alteration of the PL properties corresponding to repeated cycles of five and six coordinations triggered by the DMSO adsorption. These data clearly indicate that DMSO vapor should be captured by the tin atom, and the six-coordinate complexes were constructed, followed by luminescence. Owing to appropriate binding constants, the coordinated DMSO can be released by heating with crystal–crystal transitions. Thus, the reversible changes should be achieved. The relatively-larger difference in  $\Phi_{PL}$ s of TAZ-CF3 can be explained by the crystal packing. According to the SC-XRD data, the drastic change of intermolecular distance was revealed during the DMSO capturing and detaching (Figure 1B). Corresponding to these structural alterations, degree of electronic interaction should be varied, followed by emission efficiency changes. Optical properties of the initial samples and the first DMSO exposed ones were a little bit difference from those of the samples in the latter cycles (Figures 6 and S28, Table S15). This might be by the heat history caused in the evaporation (Figure S26). Indeed, after the first exposed samples were heated to remove DMSO, good repeatable situation was provided. The coordination number of the hypervalent tin atom can be dynamically and reversibly altered by vapor fuming. Moreover, both states can be isolated and examined by the series of analyses. Thus, optical properties at



**Figure 6.** Reversible controls of the PL properties of (A) **TAz-F** and (B) **TAz-CF3** with heating (100 °C for 30 min)-DMSO exposing (an ambient temperature for 2 h under a vapor-saturated closed condition) processes. The inserted photos show the samples irradiated by a UV lamp (365 nm).

each state can be explained. There should be almost no special electronic intermolecular interactions originating from the dimer, such as J and H-type aggregations,<sup>[69]</sup> in crystal because the variation of the optical properties including before and after DMSO attachment was similar to that in solution.

### Theoretical calculations

To support the optical properties of **TAz** complexes, density functional theory (DFT) and time-dependent (TD)-DFT calculations were executed (Figures 7, S29–S31 and Table S16). The most significant point is that the intrinsic forbidden nature of the HOMO-LUMO transition in the azobenzene ligand is changed to the allowed one by the tin coordination. The energy diagram of molecular orbitals (MOs) suggests that the  $S_0 \rightarrow S_1$  transitions of the azobenzene derivatives were assigned to the  $n \rightarrow \pi^*$  forbidden transition (oscillator strength:  $f=0.000$  for azobenzene; 0.0261 for **Az-H**). By the tin coordination, the HOMO is transformed from non-bonding MO to  $\pi$ -bonding one

by critically stabilizing the non-bonding MO (Figure 7A). As a result, the  $S_0 \rightarrow S_1$  transitions of the **TAz** complexes are assigned to the  $\pi \rightarrow \pi^*$  allowed transition ( $f=0.2354$  for **TAz-H**; 0.2316 for **TAz-H-DMSO**) (Figure 7B). These theoretical results are corresponded to the experimental data. The absorption bands from the azobenzene ligands in the longest wavelength regions were very small, meanwhile the magnitudes of these absorption bands were drastically enhanced in the **TAz** complexes (Figures 2 and S12). Moreover, the energy diagrams also proposed tin coordination caused both increase and decrease in HOMO and LUMO energy levels, respectively, in comparison to the azobenzene derivatives. From the CV data with the **TAz** complexes, these narrower energy gap effects were obviously confirmed (Figure S24 and Table S13).

To get deep insight about MO, we performed a natural bond orbital (NBO) calculation (Figures S32 and S33).<sup>[70,71]</sup> The results suggest that NBO energy levels of lone pairs of oxygen atoms (LP(O1) and LP(O2)) (for example, average energy:  $-8.05$  eV for **TAz-H**) critically increased compared to those of the methylated ligand (for example, average energy:  $-8.41$  eV

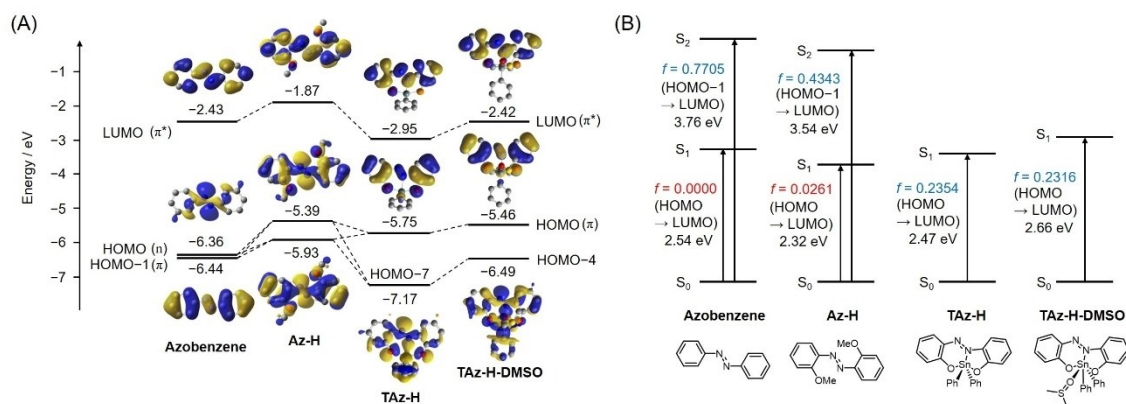


**Figure 7.** (A) Energy diagram, selected MOs and (B) oscillator strengths ( $f$ ) of selected transition bands of azobenzene, **Az-H**, **TAz-H** and **TAz-H-DMSO** obtained with DFT and TD-DFT calculations at TD-B3LYP/6-311G(d,p)//B3LYP/6-311G(d,p) level (isovalue = 0.02).

for **Az-H** (Figure S32). In other words, the electron donating ability of two oxygen atoms at the apical positions should be stronger than those of the methoxy groups owing to the 3c–4e bond character. Indeed, the contribution of 3c–4e bond was observable in HOMO-11 (bonding orbital), HOMO-7 (non-bonding orbital) and LUMO+14 (anti-bonding orbital) (Figure S34).<sup>[72]</sup> In addition, a strong donor–acceptor interaction occurred between a lone pair of nitrogen atom and the tin atom (for example, LP(N1)→LP\*(Sn1), stabilization energy: 76.35 kcal mol<sup>-1</sup> for **TAz-H**) (Figure S33), leading to decrease in the LUMO energy level. Consequently, different bond natures in the trigonal bipyramidal structure enable to coexist the two opposite properties, electron-donating and accepting abilities.

We investigated the geometry in the excited state of **TAz-H** with TD-DFT calculations (Figure S35). The **TAz-H** preserved planar structures even in the excited states in spite of elongation of nitrogen–nitrogen bonds; dihedral angle of C(1)–N(1)–N(2)–C(7) and bond length of N(1)–N(2) are 179.97° and 1.275 Å in the ground state, 179.99° and 1.327 Å in the excited state, respectively. In the previous works, we mentioned that non-planar boron-fused azomethine and azo derivatives did not show emission in solution due to intramolecular motions in the excited state.<sup>[44]</sup> Conversely, the high planarity of **TAz-H** inhibited molecular motion in the excited state, therefore we successfully received emission from the azobenzene moiety even in solution.

The TD-DFT calculation also provided speculation on the peak shifts of optical bands by the DMSO coordination. Correspondingly, hypsochromic shifts of the absorption bands were observed from the comparison with the complexes in the presence and absence of DMSO ( $\Delta E_{S_0 \rightarrow S_1} = 2.47$  eV for **TAz-H** and 2.66 eV for **TAz-H-DMSO**). Although both energy levels of HOMO and LUMO were elevated by the DMSO coordination, larger degree of increase in the LUMO energy level than that of

the HOMO was responsible for the wider energy gap. It should be mentioned that substitution effects on optical properties were good agreement with the experiment results (Figures S29 and S30).

The NBO calculation also performed with the DMSO complex. It was shown that the DMSO attachment decreased electron-accepting ability of tin atom by enhancing electron density at the tin atom (for example, LP(N1)→LP\*(Sn1), stabilization energy: 55.58 kcal mol<sup>-1</sup> for **TAz-H-DMSO**) (Figure S33). The upfield shift of the <sup>119</sup>Sn NMR signal peak by a shielding effect in DMSO-*d*<sub>6</sub> solvent experimentally supported this calculation result (Figure S2). Subsequently, the decrease in electron-accepting ability should induce elevation of LUMO and HOMO energy levels. Indeed, the energy levels of LP(O1) and LP(O2) of six coordinated geometry (for example, average energy: -7.71 eV for **TAz-H-DMSO**) were larger than those of five one (for example, average energy: -8.05 eV for **TAz-H**) (Figure S32). Considering the energy-gap relationships between **TAz-H** and **TAz-H-DMSO** as mentioned above, the LUMO energy level was effectively risen by increased electron density at the tin atom compared to the HOMO energy level. Notably, the shapes of HOMO and LUMO were preserved between five and six coordinated geometries (Figures 7A, S31). Those results are corresponded to the experimental data that the chromisms to shorter wavelength regions in both absorption and luminescence spectra can proceed through not distortion at the azobenzene moiety but drastic changes in electronic properties at the tin atom. In the **TAz** complexes, the electronic characters only at the tin atom dominate not only optical properties but also binding affinities. This is the uniqueness of this system.

Finally, we evaluated applicability of theoretical calculations for estimating binding affinity of DMSO and DMF to the tin atom (Figures 8 and S36). Accordingly, the significant linear relationship between the Sn(1)–O(3) bond length (Sn(1): **TAz**

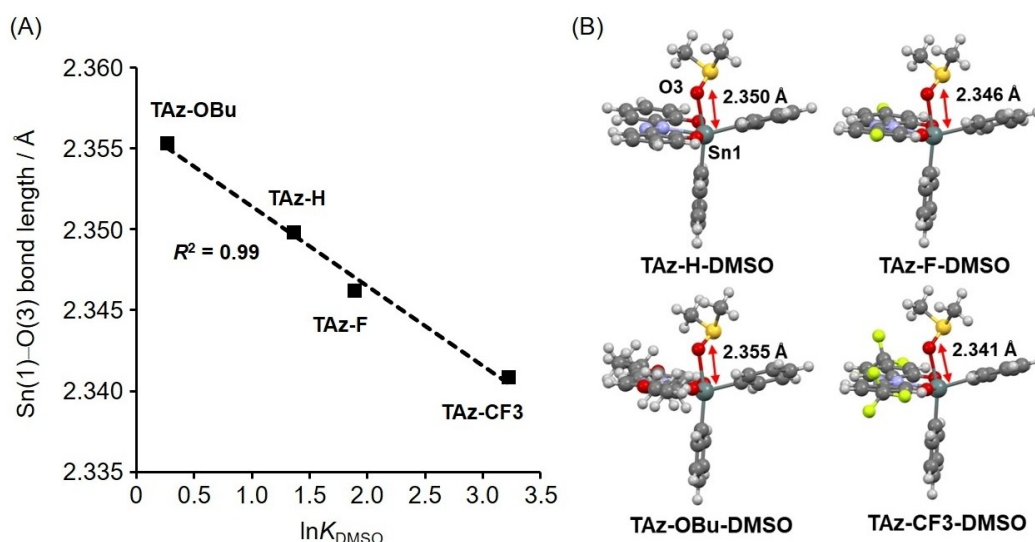


**Figure 8.** (A) The relationship between simulated Sn(1)–O(3) bond lengths of **TAz-DMSO** complexes and binding constants ( $K_{\text{DMSO}}$ ) measured in toluene solution at ambient temperature. (B) The optimized structures and simulated Sn(1)–O(3) bond lengths of **TAz-DMSO** complexes with DFT calculations at a B3LYP/6-311G(d,p) level.

complexes, O(3): DMSO or DMF) and the natural logarithm of binding constant ( $\ln K$ ) was observed. This might be based on the relationship between a Gibbs energy change and an equilibrium constant,  $\Delta G^\circ = -RT \ln K$  ( $\Delta G^\circ$ : standard Gibbs free energy change,  $R$ : universal gas constant,  $T$ : temperature). In this case, the bond length of Sn–O should be approximately proportional connection to  $\Delta G^\circ$ . Although the proof of the relationship is not clear, bond lengths might be simple parameters for the estimation of binding constants by theoretical calculation.

## Conclusion

We synthesized a series of TAz complexes having five coordinated tin atoms with the distorted trigonal bipyramidal molecular geometry. Owing to high stability of the complexes with and without solvent molecules, a series of analyses were applicable. Coexistence of electron-donating and accepting abilities originating from 3c–4e bond and Sn–N coordination, respectively, realize outstanding narrow energy gap in spite of the small azobenzene-based  $\pi$ -conjugated system. Furthermore, we found the luminochromic behaviors by the DMSO vapor fuming and subsequently by heating for the reverse process. Since dynamic and reversible shifts can proceed between five and six coordination numbers at the hypervalent tin atom, these behaviors can be obtained. From the SC-XRD and PXRD, it was revealed that the captured DMSO altered the coordination number from five to six with crystal–crystal transitions. Hypsochromic shifts of absorption and emission bands were monitored by the solvent coordination, and these optical changes were also able to be well explained by the theoretical calculation. In summary, emission color changes of  $\pi$ -conjugated systems should originate from the electronic density change at the tin atom. Our findings propose that the hypervalent system is expected to open up the field of clear vapochromic system with color-tunable  $\pi$ -conjugated system.

## Experimental Section

**Crystallographic data:** Deposition numbers 2052296, 2052299, 2052300, 2052301, 2052302, 2052305, and 2052306 contain the supplementary crystallographic data for this paper. These data are provided free of charge by the joint Cambridge Crystallographic Data Centre and Fachinformationszentrum Karlsruhe Access Structures service.

## Acknowledgements

This work was partially supported by the Inamori Foundation (for M.G.) and a Grant-in-Aid for Early-Career Scientists (for M.G.) (JSPS KAKENHI Grant numbers 20 K15334), for Scientific Research (B) (for K.T) (JP17H03067), for Challenging Research (Pioneering) (JP20 K20368), for Scientific Research on Innovative Areas “New Polymeric Materials Based on Element-Blocks (No.2401)” (JP24102013).

## Conflict of Interest

The authors declare no conflict of interest.

**Keywords:** Azobenzene · hypervalent · luminescence · tin · vapochromism

- [1] O. S. Wenger, *Chem. Rev.* **2013**, *113*, 3686–3733.
- [2] X. Zhang, B. Li, Z.-H. Chen, Z.-N. Chen, *J. Mater. Chem.* **2012**, *22*, 11427–11441.
- [3] E. Li, K. Jie, M. Liu, X. Sheng, W. Zhu, F. Huang, *Chem. Soc. Rev.* **2020**, *49*, 1517–1544.
- [4] C. Dou, L. Han, S. Zhao, H. Zhang, Y. Wang, *J. Phys. Chem. Lett.* **2011**, *2*, 666–670.
- [5] B. Prusti, M. Chakravarty, *Dyes Pigm.* **2020**, *181*, 108543.
- [6] M. Kumar, S. J. George, *Chem. Eur. J.* **2011**, *17*, 11102–11106.
- [7] Y. Akune, R. Hirose, H. Takahashi, M. Shiro, S. Matsumoto, *RSC Adv.* **2016**, *6*, 74506–74509.
- [8] S. Hatanaka, T. Ono, Y. Hisaeda, *Chem. Eur. J.* **2016**, *22*, 10346–10350.
- [9] H. Naito, Y. Morisaki, Y. Chujo, *Angew. Chem. Int. Ed.* **2015**, *54*, 5084–5087; *Angew. Chem.* **2015**, *127*, 5173–5176.
- [10] S. Ito, A. Hirose, M. Yamaguchi, K. Tanaka, Y. Chujo, *J. Mater. Chem. C* **2016**, *4*, 5564–5571.
- [11] R. Yoshii, K. Suenaga, K. Tanaka, Y. Chujo, *Chem. Eur. J.* **2015**, *21*, 7231–7237.
- [12] R. Yoshii, A. Hirose, K. Tanaka, Y. Chujo, *Chem. Eur. J.* **2014**, *20*, 8320–8324.
- [13] H. Sasaki, H. Imoto, T. Kitao, T. Uemura, T. Yumura, K. Naka, *Chem. Commun.* **2019**, *55*, 6487–6490.
- [14] K. Naka, T. Kato, S. Watase, K. Matsukawa, *Inorg. Chem.* **2012**, *51*, 4420–4422.
- [15] B. Orwat, M. J. Oh, M. Zaranek, M. Kubicki, R. Januszewski, I. Kownacki, *Inorg. Chem.* **2020**, *59*, 9163–9176.
- [16] H. Ohara, T. Ogawa, M. Yoshida, A. Kobayashi, M. Kato, *Dalton Trans.* **2017**, *46*, 3755–3760.
- [17] T. Hasegawa, A. Kobayashi, H. Ohara, M. Yoshida, M. Kato, *Inorg. Chem.* **2017**, *56*, 4928–4936.
- [18] A. Kobayashi, R. Arata, T. Ogawa, M. Yoshida, M. Kato, *Inorg. Chem.* **2017**, *56*, 4280–4288.
- [19] A. Kobayashi, K. Komatsu, H. Ohara, W. Kamada, Y. Chishina, K. Tsuge, H.-C. Chang, M. Kato, *Inorg. Chem.* **2013**, *52*, 13188–13198.
- [20] Y. Wu, X. Zhang, L.-J. Xu, M. Yang, Z.-N. Chen, *Inorg. Chem.* **2018**, *57*, 9175–9181.
- [21] J. Fornés, N. Giménez, S. Ibáñez, E. Lalinde, A. Martín, M. T. Moreno, *Inorg. Chem.* **2015**, *54*, 4351–4363.
- [22] S. Tsukamoto, S. Sakaki, *Dalton Trans.* **2013**, *42*, 4809–4821.
- [23] C. E. Strasser, V. J. Catalano, *J. Am. Chem. Soc.* **2010**, *132*, 10009–10011.
- [24] E. J. Fernández, J. M. López-de-Luzuriaga, M. Monge, M. E. Olmos, R. C. Puelles, A. Laguna, A. A. Mohamed, J. P. Fackler, *Inorg. Chem.* **2008**, *47*, 8069–8076.
- [25] E. J. Fernández, J. M. López-de-Luzuriaga, M. Monge, M. Montiel, M. E. Olmos, J. Pérez, A. Laguna, F. Mendizabal, A. A. Mohamed, J. P. Fackler, *Inorg. Chem.* **2004**, *43*, 3573–3581.
- [26] J. M. López-de-Luzuriaga, M. Monge, M. E. Olmos, J. Quintana, M. Rodríguez-Castillo, *Inorg. Chem.* **2019**, *58*, 1501–1512.
- [27] L.-Y. Zhang, L.-J. Xu, X. Zhang, J.-Y. Wang, J. Li, Z.-N. Chen, *Inorg. Chem.* **2013**, *52*, 5167–5175.
- [28] Y. Chujo, K. Tanaka, *Bull. Chem. Soc. Jpn.* **2015**, *88*, 633–643.
- [29] M. Gon, K. Tanaka, Y. Chujo, *Polym. J.* **2018**, *50*, 109–126.
- [30] K. Tanaka, Y. Chujo, *Polym. J.* **2020**, *52*, 555–566.
- [31] M. Gon, K. Sato, K. Kato, K. Tanaka, Y. Chujo, *Mater. Chem. Front.* **2019**, *3*, 314–320.
- [32] M. Gon, K. Kato, K. Tanaka, Y. Chujo, *Mater. Chem. Front.* **2019**, *3*, 1174–1180.
- [33] J. Ochi, K. Tanaka, Y. Chujo, *Angew. Chem. Int. Ed.* **2020**, *59*, 9841–9855; *Angew. Chem.* **2020**, *132*, 9925–9855.
- [34] J. Ochi, K. Tanaka, Y. Chujo, *Dalton Trans.* **2021**, *50*, 1025–1033.
- [35] S. Ohtani, Y. Takeda, M. Gon, K. Tanaka, Y. Chujo, *Chem. Commun.* **2020**, *56*, 15305–15308.
- [36] S. Ohtani, M. Gon, K. Tanaka, Y. Chujo, *Crystals* **2020**, *10*, 615.
- [37] S. Ohtani, M. Nakamura, M. Gon, K. Tanaka, Y. Chujo, *Chem. Commun.* **2020**, *56*, 6575–6578.

- [38] S. Ohtani, M. Gon, K. Tanaka, Y. Chujo, *Macromolecules* **2019**, *52*, 3387–3393.
- [39] S. Ohtani, M. Gon, K. Tanaka, Y. Chujo, *Chem. Eur. J.* **2017**, *23*, 11827–11833.
- [40] M. Gon, J. Wakabayashi, M. Nakamura, K. Tanaka, Y. Chujo, *Chem. Asian J.* **2021**, *16*, 696–703.
- [41] M. Gon, J. Wakabayashi, M. Nakamura, K. Tanaka, Y. Chujo, *Macromol. Rapid Commun.* **2021**, <https://doi.org/10.1002/marc.202000566>.
- [42] J. Wakabayashi, M. Gon, K. Tanaka, Y. Chujo, *Macromolecules* **2020**, *53*, 4524–4532.
- [43] M. Gon, J. Wakabayashi, K. Tanaka, Y. Chujo, *Chem. Asian J.* **2019**, *14*, 1837–1843.
- [44] M. Gon, K. Tanaka, Y. Chujo, *Angew. Chem.* **2018**, *130*, 6656–6661; *Angew. Chem. Int. Ed.* **2018**, *57*, 6546–6551.
- [45] M. Gon, K. Tanaka, Y. Chujo, *Chem. Rec.* **2021**, <https://doi.org/10.1002/tcr.202000156>.
- [46] J. Mei, N. L. C. Leung, R. T. K. Kwok, J. W. Y. Lam, B. Z. Tang, *Chem. Rev.* **2015**, *115*, 11718–11940.
- [47] J. Luo, Z. Xie, J. W. Y. Lam, L. Cheng, H. Chen, C. Qiu, H. S. Kwok, X. Zhan, Y. Liu, D. Zhu, B. Z. Tang, *Chem. Commun.* **2001**, 1740–1741.
- [48] Y. Dong, J. W. Y. Lam, A. Qin, Z. Li, J. Sun, H. H.-Y. Sung, I. D. Williams, B. Z. Tang, *Chem. Commun.* **2007**, 40–42.
- [49] K. E. Bessler, J. A. dos Santos, V. M. Deflon, S. de Souza Lemos, E. Niquet, *Z. Anorg. Allg. Chem.* **2004**, *630*, 742–745.
- [50] H. Preut, F. Huber, R. Barbieri, N. Bertazzi, *Z. Anorg. Allg. Chem.* **1976**, *423*, 75–82.
- [51] M. L. H. Green, G. Parkin, *Dalton Trans.* **2016**, *45*, 18784–18795.
- [52] J. Harada, K. Ogawa, *Chem. Soc. Rev.* **2009**, *38*, 2244–2252.
- [53] U. Böhme, S. Jähnigen, *Acta Crystallogr.* **2008**, *C64*, o364–o366.
- [54] A. S. Soldatenko, I. V. Sterkhova, N. F. Lazareva, *J. Organomet. Chem.* **2019**, *903*, 120997.
- [55] C. Pettinari, F. Marchetti, R. Pettinari, D. Martini, A. Drozdov, S. Troyanov, *Inorg. Chim. Acta* **2001**, *325*, 103–114.
- [56] J. S. Zugazagoitia, M. Maya, C. Damián-Zea, P. Navarro, H. I. Beltrán, J. Peon, *J. Phys. Chem. A* **2010**, *114*, 704–714.
- [57] A. Esparza-Ruiz, A. Peña-Hueso, I. Ramos-García, A. Flores-Parra, R. Contreras, *J. Organomet. Chem.* **2008**, *693*, 2739–2747.
- [58] A. Esparza-Ruiz, A. Peña-Hueso, I. Ramos-García, A. Vásquez-Badillo, A. Flores-Parra, R. Contreras, *J. Organomet. Chem.* **2009**, *694*, 269–277.
- [59] C. Camacho-Camacho, A. Esparza-Ruiz, A. Peña-Hueso, E. Mijangos, I. Ramos-García, R. Contreras, A. Flores-Parra, *Z. Anorg. Allg. Chem.* **2013**, *639*, 1122–1128.
- [60] J. Harada, K. Ogawa, S. Tomoda, *Acta Cryst. Sect. B* **1997**, *53*, 662–672.
- [61] E. Merino, M. Ribagorda, *Beilstein J. Org. Chem.* **2012**, *8*, 1071–1090.
- [62] S. A. Jenekhe, J. A. Osaheni, *Science* **1994**, *265*, 765–768.
- [63] J. Yoshino, N. Kano, T. Kawashima, *Chem. Commun.* **2007**, 559–561.
- [64] N. Singh, K. Kumar, N. Srivastav, R. Singh, V. Kaur, J. P. Jasinski, R. J. Butcher, *New J. Chem.* **2018**, *42*, 8756–8764.
- [65] J. Yoshino, A. Furuta, T. Kambe, H. Itoi, N. Kano, T. Kawashima, Y. Ito, M. Asashima, *Chem. Eur. J.* **2010**, *16*, 5026–5035.
- [66] I. P. Oliveri, G. Maccarrone, S. Di Bella, *J. Org. Chem.* **2011**, *76*, 8879–8884.
- [67] P. A. Cahill, C. E. Dykstra, J. C. Martin, *J. Am. Chem. Soc.* **1985**, *107*, 6359–6362.
- [68] Y. V. Torubaev, F. M. Dolgushin, I. V. Skabitsky, A. E. Popova, *New J. Chem.* **2019**, *43*, 12225–12232.
- [69] N. Hestand, F. C. Spano, *Chem. Rev.* **2018**, *118*, 7069–7163.
- [70] E. D. Glendening, C. R. Landis, F. Weinhold, *WIREs Comput. Mol. Sci.* **2012**, *2*, 1–42.
- [71] A. E. Reed, L. A. Curtiss, F. Weinhold, *Chem. Rev.* **1988**, *88*, 899–926.
- [72] T. Atsumi, T. Abe, K. Akiba, H. Nakai, *Bull. Chem. Soc. Jpn.* **2010**, *83*, 892–899.

---

Manuscript received: February 14, 2021

Accepted manuscript online: March 29, 2021

Version of record online: April 22, 2021